

High-purity nitrous acid (HONO) generation and quantification using broadband cavity-enhanced absorption spectroscopy (BBCEAS)

Alexis P. Harper¹, Callum E. Flowerday¹, Zachary Giauque¹, Kaitlyn Brewster¹, Ryan Thalman², Jaron C. Hansen¹

¹Brigham Young University, Department of Chemistry and Biochemistry, Provo, UT, 84602, USA

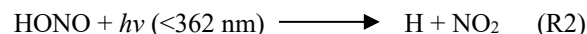
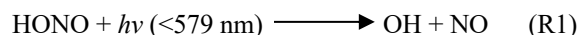
²Snow College, Department of Chemistry, Richfield, UT, 84701, USA

Correspondence to: Jaron C. Hansen (jhansen@chem.byu.edu)

Abstract. Nitrous acid (HONO) is a key atmospheric precursor to hydroxyl radicals (OH), which drive oxidation processes in the troposphere. Accurate quantification of HONO is essential for modelling atmospheric chemistry but is often challenging due to low ambient concentrations, significant wall losses from instruments with inlets, and interference from co-produced nitrogen dioxide (NO₂). Laboratory generation methods frequently struggle to produce HONO in both high purity and usable quantities. This study introduces a simple, scalable method for generating high-purity HONO via the reaction of hydrochloric acid (HCl) and sodium nitrite (NaNO₂) in a multi-bubbler system. The method incorporates a thermal “catch and release” mechanism to selectively trap HONO and separate it from NO₂ prior to analysis. While the melting point of NO₂ is well-established at -9 °C, the melting point of HONO was monitored and determined to be -4 °C, enabling the thermal separation mechanism to function effectively. Broadband cavity-enhanced absorption spectroscopy (BBCEAS) was used for detection and quantification in the 329-344 nm region. Systematic optimization of bubbler temperatures, carrier gas flow rates, capture durations, and moisture levels yielded HONO purities greater than 96%. This method enables reliable and flexible production of high-purity HONO, making it well-suited for use in laboratory-based chamber studies and instrument calibration applications.

1 Introduction

Nitrous acid (HONO) plays a pivotal role in atmospheric chemistry due to its photolysis at or below 579 nm, producing hydroxyl radicals (OH) via Reaction (R1), which initiate oxidation processes in the troposphere (Wine et al., 2020; Cox et al., 1976). At lower wavelengths, less than 362 nm, HONO photolyzes to produce NO₂ via Reaction (R2), which also contributes to oxidative processes in the troposphere (Wine et al., 2020).



HONO is introduced into the atmosphere both through direct emissions and secondary formation. Primary emissions occur from combustion processes such as biomass burning, industrial burning, domestic heating, and internal combustion engines (Pitts et al., 1984; Kurtenbach et al., 2001; Xu et al., 2015). Secondary atmospheric HONO formation involves heterogeneous reactions, including the hydrolysis of NO₂ on humid surfaces (Finlayson-Pitts et al., 2003) and NO₂ reduction by adsorbed hydrocarbons (Gutzwiller et al., 2002), as well as homogeneous gas-phase reactions and photolysis of gaseous nitrophenols. Su et al. (2011) identified soil microbial processes as a potential source of HONO through nitrite conversion. Additionally, in winter, HONO concentrations can be enhanced due to increased photolysis of nitrate in snowpacks and the presence of



35 temperature inversions, which trap pollutants near the surface, decrease vertical mixing, and extend the lifetime of precursors, promoting HONO formation pathways (Honrath et al., 2002; Beine et al., 2008; Michoud et al., 2014).

While HONO formation mechanisms vary by location, its atmospheric significance is consistently linked to its role in OH radical production. During daylight hours, HONO photolysis serves as a major source of OH, especially in the early morning when other photochemical sources like ozone (O_3) and formaldehyde (HCHO) are less active (Kleffmann et al., 2007). OH radical governs atmospheric oxidative capacity and contributes to the degradation of pollutants, influencing the formation of ground-level ozone and photochemical smog, both hazardous to human health (Elshorbany et al., 2010). Numerous studies have quantified the relative contributions of various OH initiation pathways, showing that HONO plays a major role in the lower atmosphere, even outside of urban settings (Ren et al., 2003, 2006; Elshorbany et al., 2010; Dusanter et al. 2009). Due to its importance, a comprehensive understanding of HONO sources and behaviour is essential for accurately modelling atmospheric composition and predicting pollutant lifetimes.

Reliable detection and quantification of HONO remain challenging due to interference from other nitrogen oxides and its low ambient concentrations. Various techniques, including chemiluminescence (Kanda and Taira, 1990), laser-induced fluorescence (LIF) (Bottoroff et al., 2021; Ning and Pfab, 1997), differential optical absorption spectroscopy (DOAS) (Febo et al., 1995), Fourier-transform infrared spectroscopy (FTIR) (Gingerysty and Osthoff, 2020), long path absorption photometry (LOPAP) (Heland et al., 2001; von der Heyden et al., 2022), cavity ring-down spectroscopy (CRDS) (Gingerysty and Osthoff, 2020), ultraviolet (UV) absorption (King and Moule, 1962; Stockwell and Calvert, 1978), and broadband cavity-enhanced absorption spectroscopy (BBCEAS) (Dixneuf et al., 2022; Gherman et al., 2008; Wu et al., 2012; Wu et al., 2014; Duan et al., 2018, Jordan and Osthoff, 2020), have been employed for HONO detection. Each method presents trade-offs in sensitivity, selectivity, and operational complexity.

55 In parallel, the generation of HONO in laboratory settings has been essential for calibrating instruments and simulating atmospheric processes. Traditional methods typically rely on acid displacement reactions, where a proton donor (e.g., H_2SO_4 , HCl) reacts with a nitrite salt. However, existing methods often produce significant amounts of NO_2 alongside HONO, complicating spectral quantification, particularly for spectroscopic methods where spectral overlap occurs (King and Moule, 1962; Stockwell and Calvert, 1978; Cox and Derwent, 1976). While some techniques achieve high-purity HONO, they often involve complex setups, such as the use of permeation devices, or yield low concentrations (Gingerysty and Osthoff, 2020; Reed et al., 2016; Villena and Kleffman, 2022).

Early generation methods, such as bubbling air through a solution of 0.1M sodium nitrite with 1.4-2.5% sulfuric acid, produced HONO vapours with purities around 50% (Cox and Derwent, 1976). Subsequent strategies used oxalic acid sublimed onto sodium nitrite, achieving purities of 50-90% depending on water content (Braman and De la Cantera, 1986). Flow reactor



65 designs improved stability and control, achieving >90% purity at low concentrations by dynamically mixing sulfuric acid with sodium nitrite (Taira and Kanda, 1990).

More recently, hydrochloric acid (HCl) has emerged as a viable proton donor for producing high-purity HONO via Reaction (R3).



70 Febo et al. (1995) developed a permeation-based system where HCl vapor reacted with solid NaNO_2 in a humidified gas stream, achieving HONO purities of 99.5%. Other groups have refined this concept, though some reported that HONO concentrations must remain low to avoid disproportionation (Stutz et al., 2000). This study aims to address these limitations by presenting a simple and scalable method for generating HONO using HCl as the proton donor. By thermally separating HONO from NO_2 , the method achieves high purity while producing sufficient quantities for laboratory use and experimental
75 applications.

2 Experimental

2.1 HONO generation setup

The experimental system, shown in Fig. 1, comprises a series of three bubblers immersed in controlled temperature baths. Nitrogen (N_2) serves as the carrier gas throughout the system, with tested flow rates ranging from 100-500 standard cubic
80 centimetres per minute (SCCM). The first bubbler contains 12 M HCl, while the second houses a supersaturated NaNO_2 slurry dispersed over 4 mm glass beads to maximize the surface area for the gas-phase reaction. These two bubblers are held in a constant temperature bath, with tested temperatures ranging from 20 to 40 °C. The third bubbler, the capture stage, contains dry 4 mm glass beads and is maintained in a separate temperature bath at tested temperatures ranging from -5 to -8 °C to condense and trap HONO.

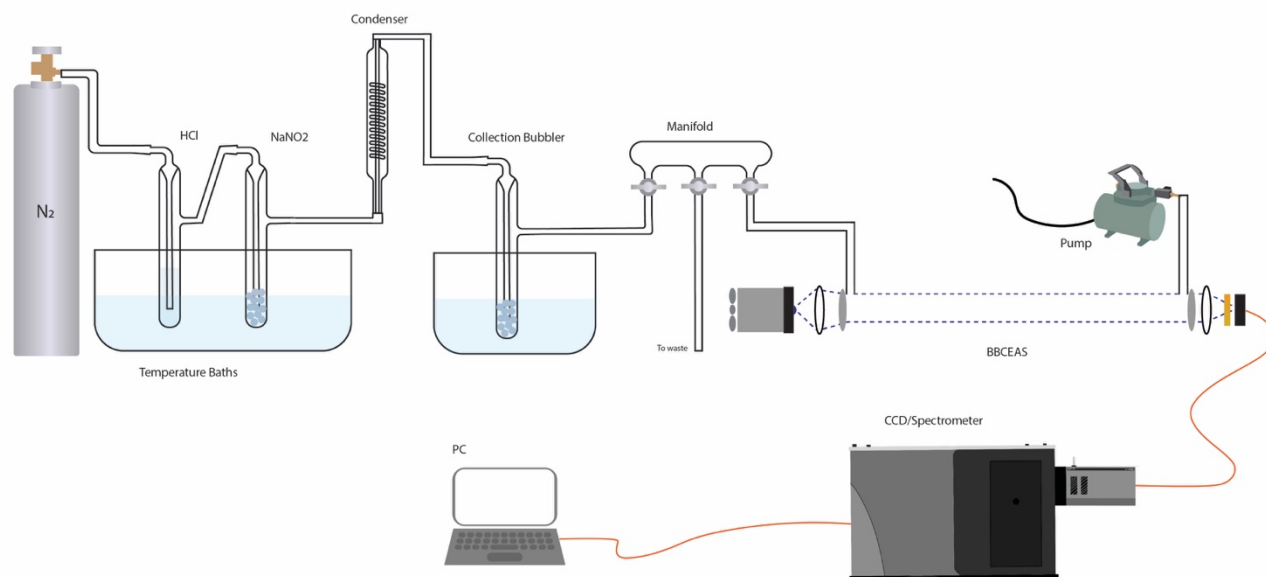


Figure 1. Nitrogen gas flows through the experimental system to produce NO_2 and HONO. HONO is captured on the final bubbler's beads, while NO_2 is passed through the manifold to waste. After the collection period, reactant bubblers are bypassed and the collection bubbler is heated up to release HONO, which flows through the BBCEAS cavity to be analysed.

Between the second and third bubblers, a condenser is set up to lower the gas mixture temperature before entering the collection bubbler. Antifreeze solution is introduced to the condenser from the collection bubbler temperature bath, making it the same temperature as the collection bubbler, which gives HONO time to cool and freeze at negative temperatures. A dilution manifold is situated between the HONO generation system and the BBCEAS cavity. During the capture phase, the manifold is directed toward waste only, allowing NO_2 to escape, while HONO is captured on the bubbler's beads. After a one-hour reaction and capture phase, the HCl and NaNO_2 bubblers are bypassed, and nitrogen is introduced at a flow rate of 1 SLM. The capture bubbler is then gradually heated to 30°C to release the trapped HONO for analysis. The manifold exit leading to the BBCEAS is then opened and allows the mixture to be diluted by a factor of two, ensuring the measured extinction falls within the instrument's linear response range and enabling accurate quantification. Adjusting the flow rate in this last step can alter the concentration of HONO exiting the system.

2.2 Thermal “catch and release” mechanism

The melting point of HONO was measured to optimize its selective capture. While the melting point of NO_2 is well-established at -9°C (O'Neil et al., 2013), HONO's melting point was identified by incrementally lowering the capture bubbler temperature and monitoring HONO release. This information guided the selection of capture temperatures that maximize HONO collection while minimizing NO_2 interference.

2.3 HONO detection using BBCEAS



105 Broadband cavity-enhanced absorption spectroscopy (BBCEAS) has been used for detection of a wide range of molecules including short chained alcohols, formaldehyde, glyoxal (CHOCHO), methyl glyoxal (CH₃COCHO) iodine oxide (IO), water vapor (H₂O), oxygen dimers (O₄), sulphur dioxide (SO₂), NO₂, and OH radical. (Thalman and Volkamer, 2010; Washenfelter et al., 2016; Thalman et al., 2022; Flowerday et al., 2023a; Flowerday et al., 2023b; Flowerday et al., 2025) Briefly, BBCEAS employs highly reflective mirrors ($R > 99.9\%$) to form an optical cavity that amplifies a 1 m base pathlength to an effective sample pathlength of 2000 m. The cavity consists of two 1" planar-concave AR-coated mirrors (Layertec 109657) mounted 1 m apart within a carbon pultruded tube cage system (Goodwinds) using 3D-printed PLA brackets. The cavity is enclosed in a brass pipe sealed against the mirrors. The light source is a UV-LED centred at 340 nm (Roithner Lasertechnik, DUV340-SD353EL-31), mounted on a copper heat sink. A Peltier cooler (Digi-Key 102-166-ND), sandwiched between the LED and heat sink and controlled by a precision temperature controller (Meerstetter TEC-1091), maintains the LED at 15 ± 0.1 °C to ensure stable light intensity. A fan is mounted on the back of the heat sink for additional thermal management. Light is guided through the cavity using UV AR-coated collimating and focusing optics (ThorLabs). A 340 ± 13 nm bandpass filter (Edmund Optics, 84092) ensures that only the desired wavelength reaches the fibre optic cable (Thorlabs BFL200HS02), which directs the light to a CCD detector cooled to -20 °C (SR-303i). For each experiment, 30 spectra with 2 s integration times were accumulated to yield one spectrum per minute. The optical setup is shown in Fig. 2.



Figure 2. The BBCEAS cavity is comprised of a broadband light source coupled into an optical cavity consisting of two highly reflective mirrors, increasing the pathlength of the light. The transmitted light is collected and directed into a spectrometer via an optical fibre, where it is dispersed and recorded using a CCD detector.

A closed cavity configuration was utilized for the BBCEAS, using a pump to pull the sample through the cavity at a rate of 2 SLM from the manifold. The known Rayleigh scattering of N₂ and He ($\epsilon_{\text{Ray,N}_2}(\lambda)$, $\epsilon_{\text{Ray,He}}(\lambda)$), along with the observed intensity drop between spectra ($I_{\text{N}_2}(\lambda)$ and $I_{\text{He}}(\lambda)$) and the distance between the mirrors (d_0), were used to calculate the reflectivity of the mirrors ($R(\lambda)$), as seen in equation 1 and Fig. 3, by flowing these gasses through the cavity directly prior to the experiment. This reflectivity value, along with the reference spectrum ($I_0(\lambda)$) and the spectrum of interest ($I(\lambda)$), was then used to determine extinction coefficients ($\epsilon(\lambda)$), as seen in equation 2, to which the known literature cross-sections of HONO and NO₂ could be fit (σ_{NO_2} , σ_{HONO}). From these fits, a concentration of the species ($[\text{NO}_2]$, $[\text{HONO}]$) could be calculated using equation 3. Using a series of concentrations over time, a total amount of HONO captured, measured in nanomoles, was



calculated for each experiment. Figure 4 shows the representative fit of experimental data to HONO and NO₂, as well as the residuals from this fit.

$$R(\lambda) = 1 - \frac{\left\{ d_0 \left(\frac{I_{\{N_2\}}(\lambda)}{I_{\{He\}}(\lambda)} \right) \left(\varepsilon_{\{Ray, N_2\}}(\lambda) - \varepsilon_{\{Ray, He\}}(\lambda) \right) \right\}}{\left\{ 1 - \left(\frac{I_{\{N_2\}}(\lambda)}{I_{\{He\}}(\lambda)} \right) \right\}} \quad (1)$$

$$\varepsilon(\lambda) = \left(\frac{\{1 - R(\lambda)\}}{\{d_0\}} + \varepsilon_{\{Ray, Air\}}(\lambda) \right) \left(\frac{\{I_0(\lambda) - I(\lambda)\}}{\{I(\lambda)\}} \right) \quad (2)$$

where I_0 is N₂, and I is our target sample.

$$\varepsilon(\lambda) = \sigma_{\{NO_2\}}[NO_2] + \sigma_{\{HONO\}}[HONO] + polynomial \dots \quad (3)$$

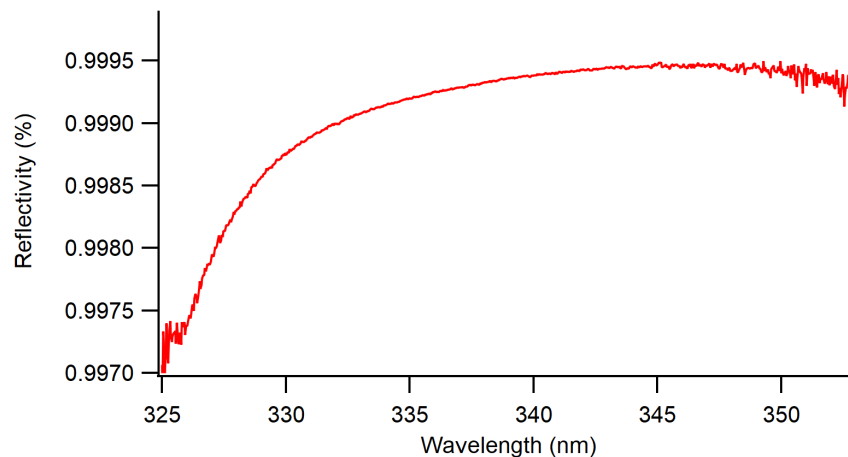


Figure 3. Reflectivity curve of mirrors. Mirrors are centered at 350 nm, where they peak at 99.95% reflectivity and the light source emits with a maximum at 330 nm, resulting in the observed overlap. Absorbance is measured between 329-344 nm, where there was sufficient light and reflectivity for detection and sensitivity.

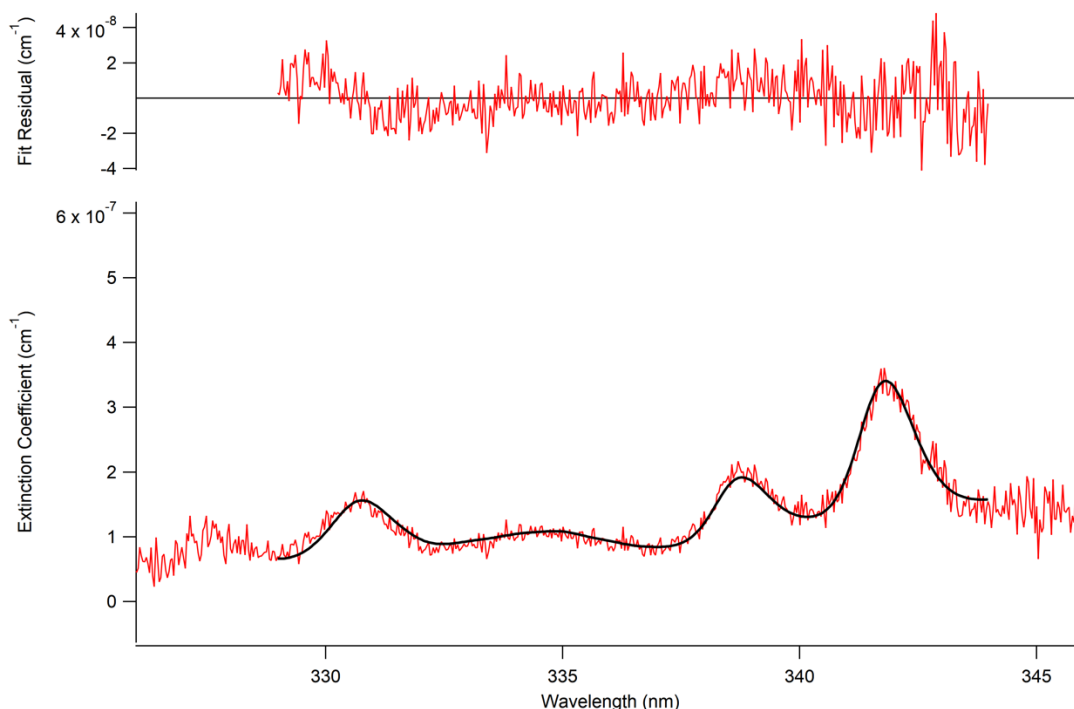


Figure 4. Fit of observed data (black) to the measured extinction coefficient (red) to determine the concentration of HONO and NO₂ in sample. Fit residual seen above.

3 Results and discussion

3.1 HONO melting point determination

The melting point of HONO was measured by monitoring its capture and subsequent release at decreasing bubbler bath temperatures. The first bath was kept constant at 30 °C as HONO and NO₂ were being generated. The second temperature bath, containing the third bubbler, temperature was stepped down incrementally until the temperature of the bath reached -10 °C, which is below the known melting point of NO₂. As seen in Fig. 5, below -4 °C, HONO recovery ceased, indicating this as the approximate melting point of HONO. NO₂, by contrast, remained in the gas phase until the bath was cooled below -9 °C. This was beneficial as it is then possible to freeze out and capture HONO, as well as allow for the majority of NO₂ to pass through the capture bubbler due to the 5 °C difference in melting points.

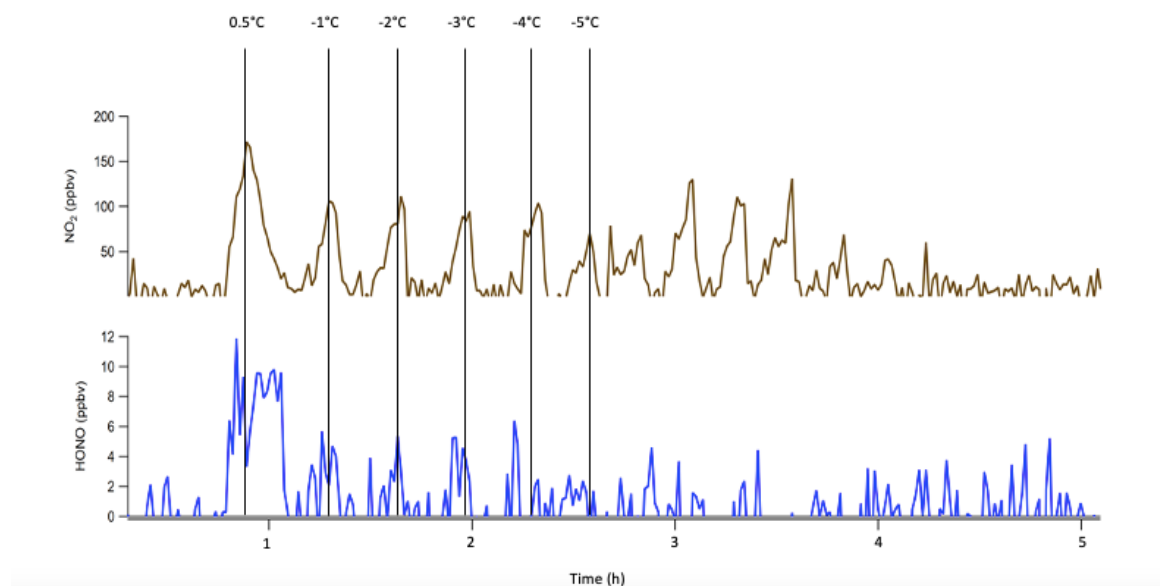


Figure 5. Concentration vs. time of NO₂ (brown) and HONO (blue) as temperature is changed incrementally over time to determine the melting point of HONO.

160 3.2 Capture bubbler optimization

Before attempting the use of the capture bubbler to further increase the purity of HONO being produced, initial tests without a capture stage yielded a HONO:NO₂ ratio of 0.46:1 (31.3% purity). This and following experiments kept a constant reactant bubbler bath temperature of 30 °C, containing the two bubblers with HCl and the NaNO₂ slurry, and a flow rate of N₂ gas through the system set at 300 SCCM. To start, the capture bubbler bath was set to –8 °C, intending to allow any excess NO₂ to pass through the system before freezing out, while HONO adhered to the beads. Implementing a capture bubbler at –8 °C improved the ratio to 2.27:1 (69.4%). Further experiments raised the temperature of the capture bubbler bath incrementally to find an optimal temperature for HONO capture. As the temperature varied, the amount of HONO captured on the beads stayed relatively constant from –8 °C to –6 °C, while purities rose, meaning less NO₂ was being captured. Purity maximized at –5.5 °C (90.4%), albeit with a slightly reduced HONO yield, decreasing from 41 nmol to 37 nmol captured. Raising the temperature beyond –5.5 °C produced similar purity of HONO, but in smaller amounts, meaning less of both HONO and NO₂ were being captured on the beads. Figure 6 shows how purity and amount of HONO changed over different capture bubbler bath temperatures.

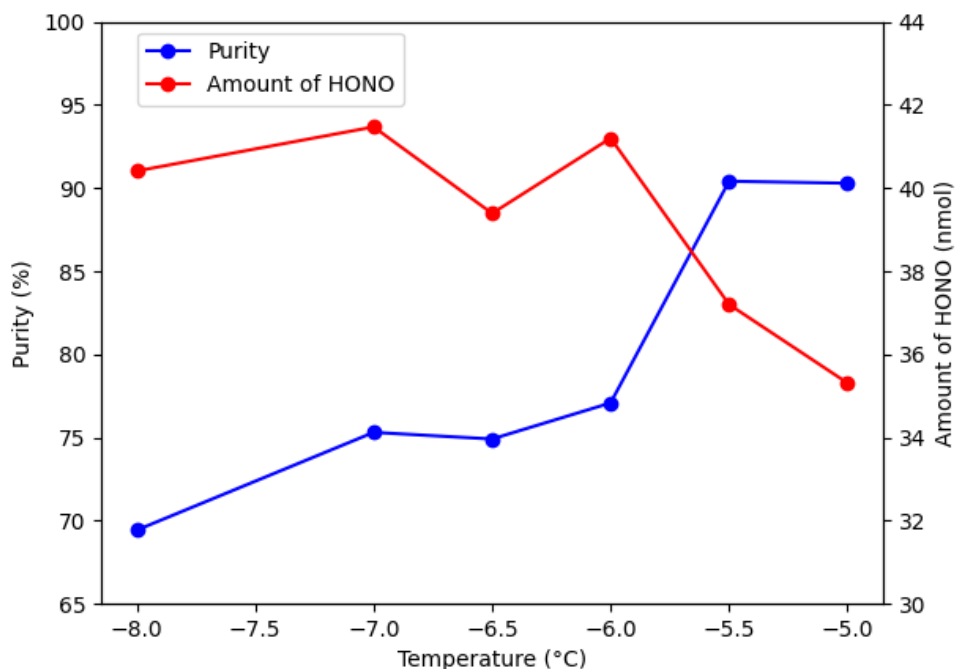


Figure 6. Effect of capture bubbler bath temperature on purity and amount of HONO.

175 3.3 Reactant bubbler bath temperature optimization

Along with capture bubbler bath temperature, the reactant bubblers' bath temperature was also changed to determine optimal HONO synthesis conditions. Different reaction bubbler temperatures will prefer HONO or NO₂ production, as temperature influences the reaction kinetics and chemical equilibria. In these experiments, the capture bubbler bath was kept constant at the optimal -5.5 °C and the flow rate remained at 300 SCCM. At 30 °C, the system produced the highest HONO purity (90.4%), with the same ratio found above (9.44:1). Figure 7 shows how purity and amount of HONO changed over different reactant bubbler bath temperatures.

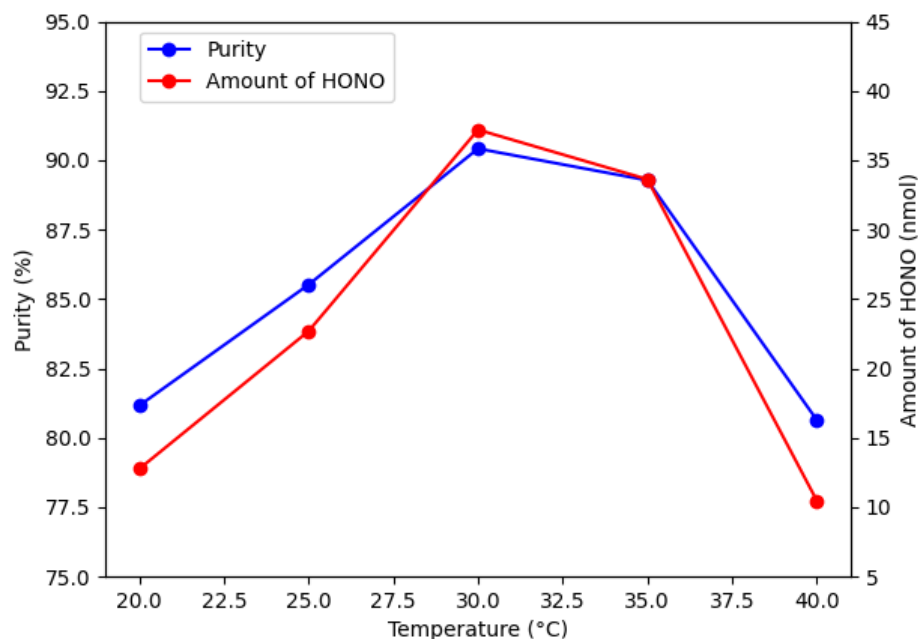


Figure 7. Effect of reactant bubbler bath temperature on purity and amount of HONO.

3.4 Carrier gas flow rate optimization

185 Lastly, the flow rate was varied to determine optimal HONO production. At lower flow rates, less HONO will be generated as less HCl gas is able to transfer to the second bubbler and react with NaNO_2 . However, once flow rates reach a certain point, N_2 gas will be moving through the bubblers too fast to transfer HCl into the NaNO_2 bubbler to be reacted. High flow rates also lead to NO_2 being pushed out of the NaNO_2 bubbler without being reacted. In these experiments, the optimal capture bubbler bath temperature of -5.5°C and reactant bubbler bath temperature of 30°C was used and the flow rate through the system was systemically varied. Flow rate experiments revealed an optimal value at 200 SCCM, yielding a HONO: NO_2 ratio of 25.53:1 (96.2% purity). Flow rates below or above this value resulted in either insufficient reaction or excess NO_2 breakthrough. Figure 8 shows how purity and amount of HONO varied with different flow rates. Figure 9 shows the concentration of HONO and NO_2 desorbed from the capture bubbler beads over time under optimal conditions of bubbler and capture temperatures, and carrier gas flow rate. Typically, it took 30-45 minutes for the glass beads to be completely desorbed of HONO and NO_2 . The more HONO and NO_2 collected, the longer the desorption process took.

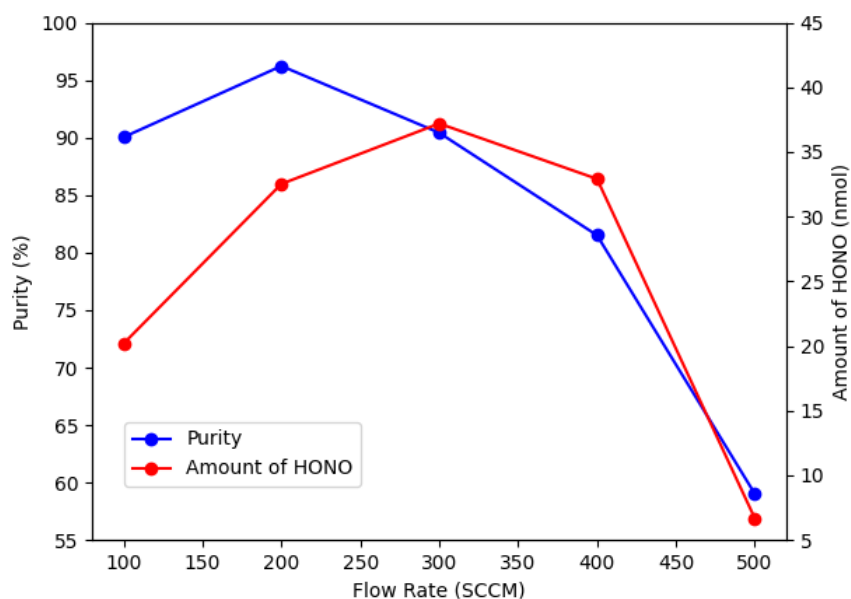


Figure 8. Effect of flow rate on purity and amount of HONO.

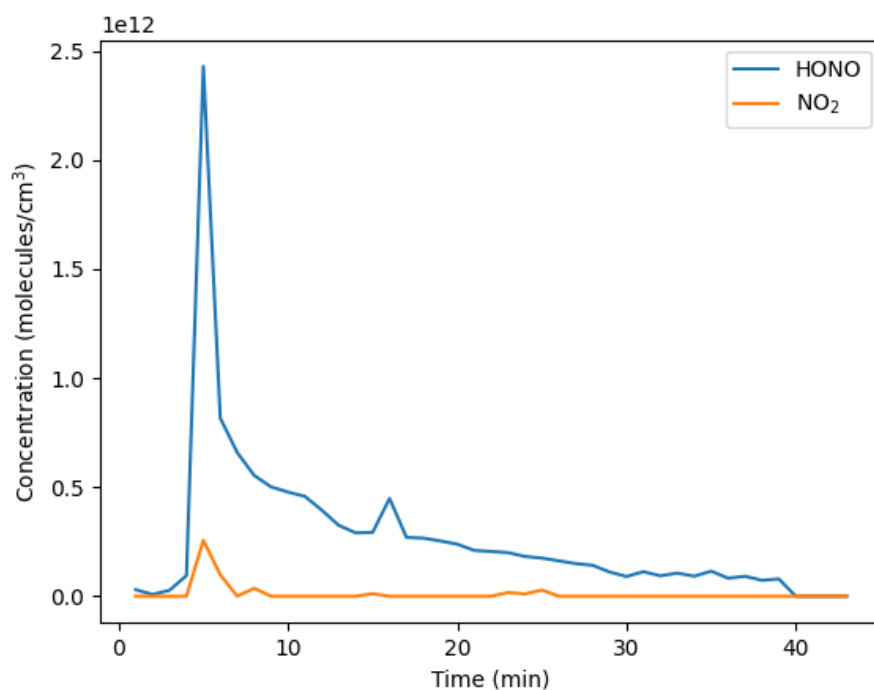


Figure 9. Concentration of HONO and NO₂ desorbing from the capture bubbler beads using the optimal HONO production method.



200 3.5 Capture duration

HONO was collected on the beads of the final bubbler for one hour in the general procedure, allowing for accurate comparison of different variables to optimize HONO production. However, extending the capture period from one to two hours under optimal conditions resulted in a higher recovery of HONO (86 nmol) without compromising purity (95.0% purity). Adjusting the collection time provides flexibility in generating specific HONO quantities. Additionally, because HONO remains stable
205 when frozen on the beads, it can be stored for later use, allowing for controlled release from the generation system by modifying the flow rate.

3.6 Moisture sensitivity

The water content of the supersaturated NaNO_2 slurry had a significant impact on product purity. Both saturated NaNO_2 solutions and dry solid NaNO_2 favoured increased NO_2 production, resulting in lower HONO purities compared to the
210 supersaturated slurry used under optimal conditions. In the optimal preparation, enough water was added to wet the NaNO_2 without fully dissolving it. Specifically, 200 g of NaNO_2 was combined with 20 mL of distilled deionized water. To assess the effect of hydration on HONO production, experiments were conducted under otherwise optimal conditions using either a saturated NaNO_2 solution or dry solid NaNO_2 . The saturated solution yielded HONO at 44.2% purity, and the solid NaNO_2 produced a mixture with 56.4% purity, both significantly lower than the 95.1% purity achieved with the supersaturated slurry.
215 These findings highlight the critical importance of precisely controlling hydration in the reaction medium.

4 Conclusions

This study presents a reproducible, scalable method for generating high-purity HONO using a multi-bubbler system with thermal separation. Through systematic optimization of bubbler temperatures, carrier gas flow, capture duration, and water content, the method achieved HONO purities exceeding 95% at high and flexible yields. The use of a thermal “catch and
220 release” system not only allows for the decoupling of HONO from interfering NO_2 , but also enables temporary storage of HONO in a condensed phase, offering flexibility in both concentration and timing of release.

This approach overcomes a longstanding limitation in acid displacement generation techniques, where NO_2 co-production often complicates spectroscopic detection and quantification. When paired with broadband cavity-enhanced absorption spectroscopy (BBCEAS), this generation method supports sensitive, selective, and high-throughput HONO detection, with
225 broad applicability in both laboratory and field-based research.

Beyond BBCEAS calibration, this technique is particularly well-suited for use in environmental chamber experiments. The ability to produce HONO at controlled purity and concentrations enables detailed studies of its role in atmospheric chemistry, including its photolysis into OH radicals, a key driver in tropospheric oxidation. Previous chamber studies such as those at



CESAM (Yi et al., 2021) and SAPHIR (Dixneuf et al., 2022) have focused primarily on HONO detection and budget analysis.
 230 CESAM has also conducted chamber studies that utilize HONO as the source for OH radical production (Lamkaddam et al.,
 2019; Picquet-Varrault et al., 2020). We present possibilities for similar chamber studies in a smaller environment,
 investigating not only HONO abundance, but also its contribution to OH formation and subsequent reaction kinetics within
 simulated atmospheric environments.

Future applications may include integration with field-deployable HONO sensors, automated sampling systems, or kinetic
 235 studies exploring the influence of HONO on radical-driven oxidation pathways. Ultimately, this method enhances our capacity
 to isolate, quantify, and mechanistically understand one of the atmosphere's most influential trace species.

References

- Beine, Harry, Agustín J. Colussi, Antonio Amoroso, Giulio Esposito, Mauro Montagnoli, and Michael R. Hoffmann. , 2008.
 "HONO Emissions from Snow Surfaces," *Environmental Research Letters* 3 (4): 045005–045005 (6).
 240 doi:10.1088/1748-9326/3/4/045005.
- Bottorff, Brandon, Emily Reidy, Levi Mielke, Sebastien Dusanter, and Philip S. Stevens. 2021. "Development of a Laser-
 Photofragmentation Laser-Induced Fluorescence Instrument for the Detection of Nitrous Acid and Hydroxyl Radicals
 in the Atmosphere." *Atmospheric Measurement Techniques* 14 (9) (Sep 16): 6039–6056. doi:10.5194/amt-14-6039-
 2021.
- 245 Braman, Robert S. and Maria A. De la Cantera. 1986. "Sublimation Sources for Nitrous Acid and Other Nitrogen Compounds
 in Air." *Anal. Chem.; (United States)* 58 (7) (Jun 1): 1533–1537. doi:10.1021/ac00298a059.
- Cox, R. A. and R. G. Derwent. 1976. "The Ultra-Violet Absorption Spectrum of Gaseous Nitrous Acid." *Journal of*
Photochemistry 6 (1) (Jan): 23–34. doi:10.1016/0047-2670(76)87004-9.
- Cox, Richard A., Richard G. Derwent, and Pauline M. Holt. 1976. "Relative Rate Constants for the Reactions of OH Radicals
 250 with H₂, CH₄, CO, NO and HONO at Atmospheric Pressure and 296 K." *Journal of the Chemical Society, Faraday*
Transactions 1: Physical Chemistry in Condensed Phases 72: 231–243. doi:10.1039/F19767202031.
- Dixneuf, Sophie, Albert A. Ruth, Rolf Häsel, Theo Brauers, Franz Rohrer, and Hans-Peter Dorn. 2022. "Detection of Nitrous
 Acid in the Atmospheric Simulation Chamber SAPHIR using Open-Path Incoherent Broadband Cavity-Enhanced
 Absorption Spectroscopy and Extractive Long-Path Absorption Photometry." *Atmospheric Measurement*
 255 *Techniques* 15 (4) (Feb 23): 945–964. doi:10.5194/amt-15-945-2022.
- Duan, Jun, Min Qin, Bin Ouyang, et al. 2018. "Development of an Incoherent Broadband Cavity-Enhanced Absorption
 Spectrometer for in Situ Measurements of HONO and NO₂." *Atmospheric Measurement Techniques* 11 (7) (Jul 30):
 4531–4543. doi:10.5194/amt-11-4531-2018.



- Dusanter, S., D. Vimal, P. S. Stevens, et al. 2009. "Measurements of OH and HO₂ concentrations during the MCMA-2006
 260 Field Campaign - Part 2: Model Comparison and Radical Budget." *Atmospheric Chemistry and Physics* 9 (18) (Sep 15): 6655–6675.
- Elshorbany, Yasin, Ian Barnes, Karl H. Becker, Jörg Kleffmann, and Peter Wiesen. 2010. "Sources and Cycling of
 Tropospheric Hydroxyl Radicals – an Overview." *Zeitschrift Für Physikalische Chemie (Neue Folge)* 224 (7) (Aug
 1): 967–987. doi:10.1524/zpch.2010.6136.
- 265 Febo, Antonio, Cinzia Perrino, Monica Gherardi, and Roberto Sparapani. 1995. "Evaluation of a High-Purity and High-
 Stability Continuous Generation System for Nitrous Acid." *Environmental Science & Technology* 29 (9) (Sep 1):
 2390–2395. doi:10.1021/es00009a035.
- Finlayson-Pitts, B. J., L. M. Wingen, A. L. Sumner, D. Syomin, and K. A. Ramazan. 2003. "The Heterogeneous Hydrolysis
 of NO₂ in Laboratory Systems and in Outdoor and Indoor Atmospheres: An Integrated Mechanism." *Physical
 270 Chemistry Chemical Physics* 5 (2) (Jan 2): 223–242. doi:10.1039/b208564j.
- Flowerday, Callum E., Nitish Bhardwaj, Ryan Thalman, Matthew C. Asplund, Eric T. Sevy, and Jaron C. Hansen. , 2023a.
 "Absorption Cross-Sections for the 5th and 6th Vibrational Overtones in a Series of Short Chained Alcohols using
 Incoherent Broadband Cavity Enhanced-Absorption Spectroscopy (IBBCEAS)," *Journal of Molecular
 Spectroscopy* 392: 111746. doi:10.1016/j.jms.2023.111746.
- 275 Flowerday, Callum E., Ryan Thalman, Matthew C. Asplund, and Jaron C. Hansen. 2023b. "Broadband Cavity-Enhanced
 Absorption Spectroscopy (BBCEAS) Coupled with an Interferometer for on-Band and Off-Band Detection of
 Glyoxal." *Toxics (Basel)* 12 (1) (Dec 28): 26. doi:10.3390/toxics12010026.
- Flowerday, Callum E., Ryan Thalman, Matthew C. Asplund, et al. 2025. "Open Path Spectroscopic Detection of Hydroxyl
 Radical: A Comparison between Broadband Cavity-Enhanced Absorption Spectroscopy (BBCEAS) and BBCEAS
 280 Coupled with a Fabry-Pérot Interferometer (BBCEAS-FP)." *Analytical Chemistry (Washington)* 97 (22) (Jun 10):
 11831. doi:10.1021/acs.analchem.5c01515.
- Gherman, Titus, Dean S. Venables, Stewart Vaughan, Johannes Orphal, and Albert A. Ruth. 2008. "Incoherent Broadband
 Cavity-Enhanced Absorption Spectroscopy in the Near-Ultraviolet: Application to HONO and NO₂." *Environmental
 Science & Technology* 42 (3) (Feb 1): 890–895. doi:10.1021/es0716913.
- 285 Gingerysty, Nicholas J. and Hans D. Osthoff. 2020. "A Compact, High-Purity Source of HONO Validated by Fourier
 Transform Infrared and Thermal-Dissociation Cavity Ring-Down Spectroscopy." *Atmospheric Measurement
 Techniques* 13 (8) (Aug 5): 4159–4167. doi:10.5194/amt-13-4159-2020.
- Gutzwiller, Lukas, Frank Arens, Urs Baltensperger, Heinz W. Gäggeler, and Markus Ammann. 2002. "Significance of
 Semivolatile Diesel Exhaust Organics for Secondary HONO Formation." *Environmental Science & Technology* 36
 290 (4) (Feb 15): 677–682. doi:10.1021/es015673b.



- Heland, Jörg, Jörg Kleffmann, Ralf Kurtenbach, and Peter Wiesen. , 2001. "A New Instrument to Measure Gaseous Nitrous Acid (HONO) in the Atmosphere," *Environmental Science & Technology* 35 (15): 3207–3212. doi:10.1021/es000303t.
- 295 Honrath, R. E., Y. Lu, M. C. Peterson, et al. , 2002. "Vertical Fluxes of NO_x, HONO, and HNO₃ Above the Snowpack at Summit, Greenland," *Atmospheric Environment (1994)* 36 (15-16): 2629–2640. doi:10.1016/S1352-2310(02)00132-2.
- Jordan, Nick and Hans D. Osthoff. 2020. "Quantification of Nitrous Acid (HONO) and Nitrogen Dioxide (NO₂) in Ambient Air by Broadband Cavity-Enhanced Absorption Spectroscopy (IBBCEAS) between 361 and 388 nm." *Atmospheric Measurement Techniques* 13 (1) (Jan 23): 273–285. doi:10.5194/amt-13-273-2020.
- 300 Kanda, Yukio and Masafumi Taira. 1990. "Chemiluminescent Method for Continuous Monitoring of Nitrous Acid in Ambient Air." *Analytical Chemistry* 62 (19) (Oct 1): 2084–2087. doi:10.1021/ac00218a007.
- King, G. W. and D. Moule. 1962. "The Ultraviolet Absorption Spectrum of Nitrous Acid in the Vapor State." *Canadian Journal of Chemistry* 40 (11) (Nov 1): 2057–2065. doi:10.1139/v62-316.
- Kleffmann, Jörg. 2007. "Daytime Sources of Nitrous Acid (HONO) in the Atmospheric Boundary Layer." *ChemPhysChem* 8 (8) (Jun 4): 1137–1144. doi:10.1002/cphc.200700016.
- 305 Kurtenbach, R., K. H. Becker, J. A. G. Gomes, et al. 2001. "Investigations of Emissions and Heterogeneous Formation of HONO in a Road Traffic Tunnel." *Atmospheric Environment (1994)* 35 (20) (Jul 1): 3385–3394. doi:10.1016/S1352-2310(01)00138-8.
- Lamkaddam, Houssni, Aline Gratien, Manon Ropion, Edouard Pangui, and Jean-François Doussin. , 2019. "Kinetic Study of the Temperature Dependence of OH-Initiated Oxidation of n-Dodecane," *The Journal of Physical Chemistry. A, Molecules, Spectroscopy, Kinetics, Environment, & General Theory* 123 (44): 9462–9468. doi:10.1021/acs.jpca.9b07704.
- 310 Michoud, V., A. Colomb, A. Borbon, et al. , 2014. "Study of the Unknown HONO Daytime Source at a European Suburban Site during the MEGAPOLI Summer and Winter Field Campaigns," *Atmospheric Chemistry and Physics* 14 (6): 2805–2822. doi:10.5194/acp-14-2805-2014.
- 315 Ning, C. L. and J. Pfab. 1997. "Generation and 355 Nm Laser Photodissociation of Nitrous Acid (HONO) and HONO–Water Clusters." *The Journal of Physical Chemistry. A, Molecules, Spectroscopy, Kinetics, Environment, & General Theory* 101 (34) (Aug 21): 6008–6014. doi:10.1021/jp9711712.
- O'Neil, Maryadele J., Patricia E. Heckelman, Peter H. Dobbelaar, Kristin J. Roman, Catherine M. Kenny, and Linda S. Karaffa. 2013. *The Merck Index : An Encyclopedia of Chemicals, Drugs, and Biologicals*. Fifteenth edition. ed. The Royal Society of Chemistry.
- 320 Picquet-Varrault, Bénédicte, Ricardo Suarez-Bertoa, Marius Duncianu, et al. , 2020. "Photolysis and Oxidation by OH Radicals of Two Carbonyl Nitrates: 4-Nitrooxy-2-Butanone and 5-Nitrooxy-2-Pentanone," *Atmospheric Chemistry and Physics* 20 (1): 487–498. doi:10.5194/acp-20-487-2020.



- 325 Pitts, James N., Heinz W. Biermann, Arthur M. Winer, and Ernesto C. Tuazon. 1984. "Spectroscopic Identification and Measurement of Gaseous Nitrous Acid in Dilute Auto Exhaust." *Atmospheric Environment* (1967) 18 (4): 847–854. doi:10.1016/0004-6981(84)90270-1.
- Reed, Chris, Charlotte A. Brumby, Leigh R. Crilley, et al. 2016. "HONO Measurement by Differential Photolysis." *Atmospheric Measurement Techniques* 9 (6) (Jun 7): 2483–2495. doi:10.5194/amt-9-2483-2016.
- 330 Ren, X. 2003. "OH and HO₂ Chemistry in the Urban Atmosphere of New York City." *Atmospheric Environment* 37 (26) (Aug 1): 3639–3651. doi:10.1016/s1352-2310(03)00459-x.
- Ren, Xinrong, William H. Brune, Jingqiu Mao, et al. 2006. "Behavior of OH and HO₂ in the Winter Atmosphere in New York City." *Atmospheric Environment* 40: 252–263. doi:10.1016/j.atmosenv.2005.11.073.
- Stockwell, William R. and Jack G. Calvert. 1978. "The Near Ultraviolet Absorption Spectrum of Gaseous HONO and
 335 N₂O₃." *Journal of Photochemistry* 8 (2) (Jan): 193–203. doi:10.1016/0047-2670(78)80019-7.
- Stutz, J., E. S. Kim, U. Platt, P. Bruno, C. Perrino, and A. Febo. 2000. "UV-Visible Absorption Cross Sections of Nitrous Acid." *Journal of Geophysical Research, Washington, DC* 105 (D11) (Jun 16): 14585–14592. doi:10.1029/2000JD900003.
- Su, Hang, Yafang Cheng, Robert Oswald, et al. 2011. "Soil Nitrite as a Source of Atmospheric HONO and OH
 340 Radicals." *Science* 333 (6049) (Sep 16): 1616–1618. doi:10.1126/science.1207687.
- Taira, Masafumi and Yukio Kanda. 1990. "Continuous Generation System for Low-Concentration Gaseous Nitrous Acid." *Analytical Chemistry (Washington)* 62 (6) (Mar 15): 630–633. doi:10.1021/ac00205a018.
- Thalman, R. and R. Volkamer. 2010. "Inherent Calibration of a Blue LED-CE-DOAS Instrument to Measure Iodine Oxide, Glyoxal, Methyl Glyoxal, Nitrogen Dioxide, Water Vapour and Aerosol Extinction in Open Cavity
 345 Mode." *Atmospheric Measurement Techniques* 3 (6) (Jan 1): 1797–1814. doi:10.5194/amt-3-1797-2010.
- Thalman, Ryan, Nitish Bhardwaj, Callum E. Flowerday, and Jaron C. Hansen. 2022. "Detection of Sulfur Dioxide by Broadband Cavity-Enhanced Absorption Spectroscopy (BBCEAS)." *Sensors (Basel, Switzerland)* 22 (7) (Mar 29): 2626. doi:10.3390/s22072626.
- Villena, Guillermo and Jörg Kleffmann. 2022. "A Source for the Continuous Generation of Pure and Quantifiable HONO
 350 Mixtures." *Atmospheric Measurement Techniques* 15 (3) (Feb 8): 627–637. doi:10.5194/amt-15-627-2022.
- von der Heyden, Lisa, Walter Wißdorf, Ralf Kurtenbach, and Jörg Kleffmann. , 2022. "A Relaxed Eddy Accumulation (REA) LOPAP System for Flux Measurements of Nitrous Acid (HONO)," *Atmospheric Measurement Techniques* 15 (6): 1983–2000. doi:10.5194/amt-15-1983-2022.
- Washenfelder, R. A., A. R. Attwood, J. M. Flores, K. J. Zarzana, Y. Rudich, and S. S. Brown. 2016. "Broadband Cavity-
 355 Enhanced Absorption Spectroscopy in the Ultraviolet Spectral Region for Measurements of Nitrogen Dioxide and Formaldehyde." *Atmospheric Measurement Techniques* 9 (1) (Jan 15): 41–52. doi:10.5194/amt-9-41-2016.



- Wine, P. H., D. M. Wilmouth, C. J. Percival, et al. 2020. *Chemical Kinetics and Photochemical Data for use in Atmospheric Studies; Evaluation Number 19*. Jet Propulsion Laboratory: Pasadena, CA: Jet Propulsion Laboratory, National Aeronautics and Space Administration, 2020.
- 360 Wu, T., W. Chen, E. Fertein, F. Cazier, D. Dewaele, and X. Gao. 2012. "Development of an Open-Path Incoherent Broadband Cavity-Enhanced Spectroscopy Based Instrument for Simultaneous Measurement of HONO and NO₂ in Ambient Air." *Applied Physics. B, Lasers and Optics* 106 (2) (Feb): 501–509. doi:10.1007/s00340-011-4818-3.
- Wu, Tao, Qiaozhi Zha, Weidong Chen, Zheng Xu, Tao Wang, and Xingdao He. 2014. "Development and Deployment of a Cavity Enhanced UV-LED Spectrometer for Measurements of Atmospheric HONO and NO₂ in Hong Kong." *Atmospheric Environment (1994)* 95 (Oct 1): 544–551. doi:10.1016/j.atmosenv.2014.07.016.
- 365 Xu, Zheng, Tao Wang, Jueqi Wu, et al. 2015. "Nitrous Acid (HONO) in a Polluted Subtropical Atmosphere: Seasonal Variability, Direct Vehicle Emissions and Heterogeneous Production at Ground Surface." *Atmospheric Environment* 106 (Apr): 100–109. doi:10.1016/j.atmosenv.2015.01.061.
- Yi, Hongming, Mathieu Cazaunau, Aline Gratien, et al. 2021. "Intercomparison of IBBCEAS, NitroMAC and FTIR Analyses for HONO, NO₂ and CH₂O Measurements during the Reaction of NO₂ with H₂O Vapour in the Simulation Chamber CESAM." *Atmospheric Measurement Techniques* 14 (8) (Aug 20): 5701–5715. doi:10.5194/amt-14-5701-2021.
- 370